ISSN 1029-9599, Physical Mesomechanics, 2021, Vol. 24, No. 6, pp. 684–691. © Pleiades Publishing, Ltd., 2021.
Russian Text © The Author(s), 2021, published in Fizicheskaya Mezomekhanika, 2021, Vol. 24, No. 4, pp. 64–72.

Synthesis of TaNbHfZrW-Based Nanopowders by Thermolysis of Transition Metal Halides in the Form of Dry Mixtures and Gels

S. Vorotylo[1], A. S. Sedegov[1], K. V. Vorotylo[1], and D. O. Moskovskikh[1]*

[1] *National University of Science and Technology MISIS, Moscow, 119049 Russia*
** e-mail: mos@misis.ru, dmitry.moskovskikh@gmail.com*

Received May 17, 2021; revised June 09, 2021; accepted June 09, 2021

Abstract—High-entropy alloys and ceramics as a new class of materials containing five or more elements are attracting increasing interest due to their unique structure and potential applications. In this work, we investigate the feasibility of the combustion synthesis of high-entropy alloys and ceramics in the Ta–Nb–Hf–Zr–W–Mg and Ta–Nb–Hf–Zr–W–Cl–Mg–N systems from chloride precursors. To this end, we analyzed the stability of metallic, chloride, nitride and hydride phases in the 0–2000°C temperature interval by varying the chemical potentials of the gaseous elements (chlorine and nitrogen). Two synthesis methods were developed: combustion of powder mixtures of transition metal chlorides with the reducing agent (Mg_3N_2), and combustion of gel mixtures. Combustion of the powder mixtures produced highly porous sinter cakes consisting of needle-like nanoparticles of high-entropy Ta + Nb + Hf + Zr + W alloy in the matrix of magnesium oxychloride. Combustion of the gels yielded spherical nanopowders with uniform composition and particle size. However, high reactivity of the synthesized powders led to their rapid oxidation due to the abundance of oxygen in the gel-forming agent (C_2H_5OH).

Keywords: high-entropy alloys, high-entropy ceramics, nitride, nanopowder, self-propagating high-temperature synthesis, solution combustion synthesis, metallothermic reduction

DOI: 10.1134/S1029959921060060

1. INTRODUCTION

A rapidly growing number of investigations into high-entropy materials is explained by the theoretical predictions that they should have improved properties as compared to conventional materials, and these assumptions have already found a lot of confirmation. High-entropy materials were shown to exhibit unique mechanical properties from cryogenic to high temperatures, fatigue strength and abrasion resistance [1, 2], considerable tensile strength [3], impact strength [4], etc. Some of these properties are probably associated with nanotwinning in high-entropy materials [5]. Another property of these alloys is exceptional resistance to grain growth, providing the formation of nanocrystalline materials [6]. High-entropy alloys have already found practical applications as structural materials, binders in cermets, etc. [7–9]. The currently available methods of production of high-entropy materials are melt crystallization, mechanical alloying, and vacuum deposition. New methods and approaches are being searched for. The aim of this work is to present modern synthesis technologies for high-entropy materials. We report new promising methods for producing nanopowders of five-component TaNbHfZrW high-entropy alloy and (TaNbHfZrW)N high-entropy ceramics with uniform composition and particle size. The proposed approaches combine solution combustion synthesis [10–12] and reduction of metals from the salt mixture using self-propagating high-temperature synthesis (SHS) [13, 14].

The method of solution combustion synthesis has gained extraordinary popularity due to its versatility (thousands of binary and multicomponent compounds were thus synthesized), simplicity of the equipment used, short synthesis time, and minimum energy consumption [15]. Until recently, only oxide materials were thus prepared. However, latest studies show the possibility of synthesizing nanopowders of metals Ni, Co, Cu, Pt [16] and Ni-Fe alloys [17, 18].

In this work, the mixing of five transition metal chlorides $TaCl_5 + NbCl_5 + HfCl_4 + ZrCl_4 + WCl_6$ with urotropine and magnesium nitride yields a highly dispersed composite precursor, which is subsequently combusted in a nitrogen atmosphere. The use of five metallic elements significantly increases the configurational entropy [11]. A similar situation is true in metallothermic reduction of transition metal halides occurring in a combustion wave. No publications on this subject are currently available.

2. MATERIALS AND METHODS

As the starting reagents we use tantalum pentachloride, hafnium tetrachloride (pure grade), zirconium tetrachloride (pure grade), niobium pentachloride (pure grade), tungsten hexachloride (pure grade), urotropine (reagent grade), MPF-1 magnesium powder, chips of high-purity magnesium (with the impurity content <0.001%; American Elements), and gaseous nitrogen (pure grade). Magnesium nitride used as the reducing agent is prepared by annealing magnesium chips in nitrogen flow at the temperature 900°C for 3 h. The nitrogen flow rate is 2 L/min.

Synthesis is performed in the following reaction compositions:

(1) reaction powder mixture $(TaCl_5 + NbCl_5 + HfCl_4 + ZrCl_4 + WCl_6) + Mg_3N_2$,

(2) gel prepared by dissolving the $TaCl_5 + ZrCl_4 + WCl_6 + HfCl_4 + NbCl_5 + 5Mg_3N_2$ powder mixture in ethanol,

(3) gel prepared by dissolving the $TaCl_5 + ZrCl_4 + WCl_6 + HfCl_4 + NbCl_5 + 5Mg_3N_2 + 0.2C_6H_{12}N_4$ powder mixture in ethanol.

Powder mixtures are ground and mixed either in a ceramic mortar, or a BML-2 ball mill (DAIHAN Scientific, South Korea), or a C2.0 Turbula mixer (Vibrotechnik, Russia). The steel cylinders of the ball mill have the volume 250 mL and rotate at a controlled speed; the ball-to-powder ratio is 20 : 1. The Turbula mixer has a steel cylinder 3 L in volume and steel balls with the ball-to-powder ratio 1 : 1.

For combustion tests, the prepared mixtures are compacted into cylindrical specimens 10 mm in diameter and 16–20 mm in height with the relative density 55–60%. A specimen is mounted on the holder made of boron nitride, and the TR5/TR20 microthermocouple is installed in a hole preliminary drilled in the specimen. A tungsten wire coil is pressed to the specimen surface. Then, the holder and the specimen are placed in a laboratory SHS reactor 5 L in volume, which is evacuated and filled with argon. Combustion is initiated by heating the tungsten coil. The combustion process is recorded by a Panasonic WVBL600 high-speed video camera at 15x magnification with a darkening filter. Temperature on the thermocouple is recorded through an analog-to-digital converter. The temperature measurement error is 10–50°C.

Gel is prepared by dissolving the chloride precursor in ethanol and introducing, into the resulting solution, the magnesium nitride powder mechanically activated in nitrogen for 20 min. In contrast to the conventional solution combustion, where both the fuel and the metal source are dissolved, in the developed synthesis method the reducing agent is insoluble in ethanol and remains in the solid state. A promising reducing agent is magnesium nitride because this brittle compound does not decompose during grinding and does not form a ductile metal in contrast to calcium hydride. Magnesium nitride is subjected to high-energy mechanical treatment (mechanical activation) to provide a sufficient dispersion for a suspension to form, which will be fixed in the viscous gel upon evaporation of the solution (according to the Stokes law). A large area of the specific reaction surface is thus ensured, which is necessary to obtain homogeneous products. The resulting gel is combusted in a tube furnace in the overall combustion mode at 900°C in the flow of argon or nitrogen.

The microstructure of nanopowders is viewed through an S-3400 N scanning electron microscope (Hitachi, Japan) with a NORAN energy dispersive attachment. The phase composition is studied by the X-ray diffraction method on a D2 PHASER diffractometer (Bruker AXS GmbH, Germany) using Cu-K_α radiation. The specific surface area of products is measured by the Brunauer–Emmett–Teller (BET) method using a NOVA 1200 setup (Quantachrome Instruments, United States); before analysis, the specimens are degassed at 200°C for 15 h. Thermodynamic calculations are performed using HSC Chemistry 6.5 and Materials Project API software.

3. RESULTS AND DISCUSSION

3.1. Calculation of Phase Stability and Possible Mechanisms of Phase Formation

Table 1 shows the calculation results for the stability of metal phases in the presence of nitrogen and chlorine. From the tabulated data, it can be seen that magnesium most easily combines with chlorine, and magnesium chloride is much more stable than its nitride. This leads to exchange reactions in a combus-

Table 1. Stability of metals in the presence of nitrogen and chlorine

Metal element	Chemical potential of nitrogen (μN) at which a metal (not its nitrides) is stable, eV	Chemical potential of chlorine (μCl), at which a metal (not its chlorides) is stable, eV
Hf	<–12.067	<–4.14
Ta	<–11.086	<–4.013
W	<–9.505	<–3.276
Mg	<–10.294	<–4.641
Nb	<–11.405	<–3.758
Zr	<–11.98	<–4.622

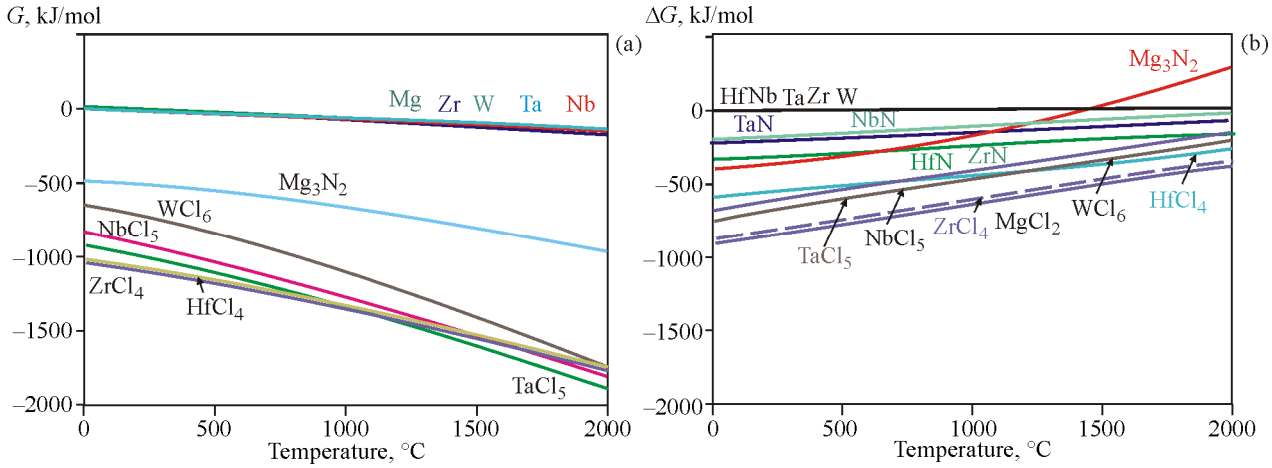

Fig. 1. Gibbs free energy G (a) and Gibbs energy differential ΔG (b) for the $(TaCl_5 + NbCl_5 + HfCl_4 + ZrCl_4 + WCl_6) + Mg_3N_2$ powder mixture in the temperature interval 0–2000°C (color online).

tion wave, resulting in the decomposition of magnesium nitride, the release of gaseous nitrogen, and the formation of magnesium chloride.

Figure 1 shows values of the Gibbs free energy G and Gibbs energy differential ΔG for a system with a constant number of particles at the SHS of the mixture of higher chlorides of tantalum, niobium, hafnium, zirconium, and tungsten with the reducing magnesium nitride. Solid lines correspond to experimental values; dashed lines, to projections. At elevated temperatures, the Gibbs energy differential of the magnesium nitride becomes positive, while the Gibbs energy differential of the metallic elements remains zero (Fig. 1b). This shifts the system equilibrium towards the formation of magnesium chloride upon the interaction of magnesium nitride with zirconium and hafnium chlorides.

3.2. Experiments on Combustion Synthesis of Mechanically Activated Dry Mixtures

Figure 2a shows a thermogram of combustion of a mechanically activated $(TaCl_5 + NbCl_5 + HfCl_4 + ZrCl_4 +$

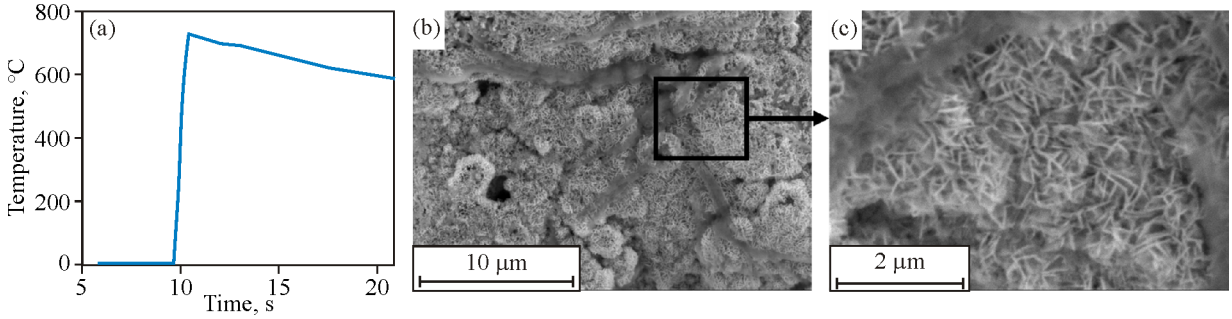

Fig. 2. Thermogram of combustion of the $(TaCl_5 + NbCl_5 + HfCl_4 + ZrCl_4 + WCl_6) + Mg_3N_2$ mixture (a); microstructures of combustion products (b, c) (color online).

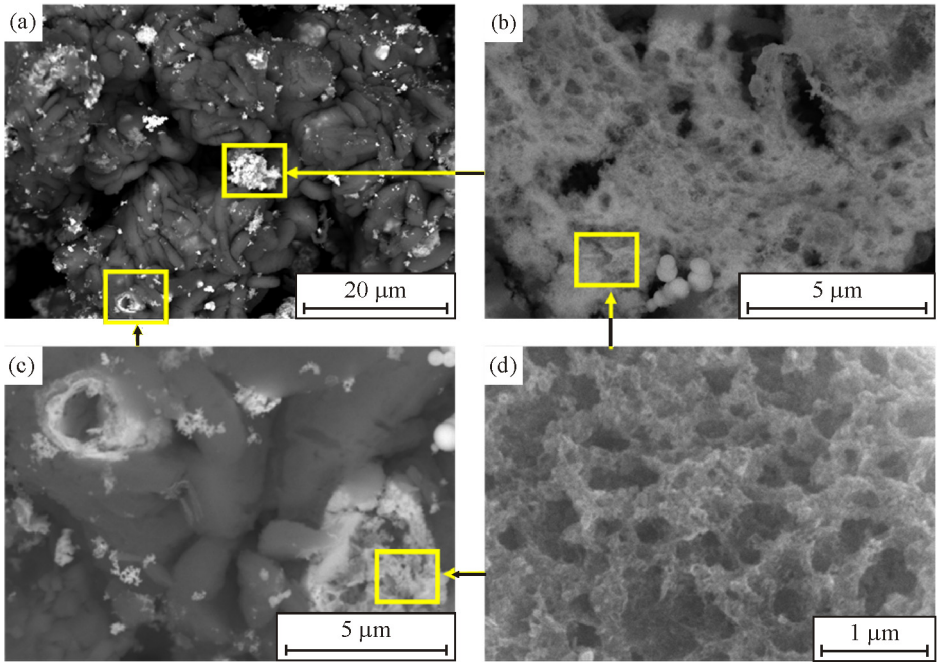

Fig. 3. Combustion products of the $TaCl_5 + ZrCl_4 + WCl_6 + HfCl_4 + NbCl_5 + 5Mg_3N_2$ mixture at 900°C in argon.

$WCl_6) + Mg_3N_2$ mixture. The maximum temperature in the combustion front is seen to be about 750°C. Scanning electron microscopy and energy dispersive X-ray spectroscopy disclose the formation of two main phases in combustion products, namely, magnesium chloride $MgCl_2$ and high-entropy TaNbHfZrW alloy (Fig. 2b). These high-entropy alloys have an acicular structure, with particles being shaped to needles up to 600 nm in length and up to 100 nm in thickness (Fig. 2c).

During combustion of $TaCl_5 + ZrCl_4 + WCl_6 + HfCl_4 + NbCl_5 + 5Mg_3N_2$ mixtures in argon, the reaction products contain tortuous porous structures, with magnesium oxychloride in the outer layer and metal agglomerates in the inner layer (Figs. 3a and 3b). High-resolution SEM (Figs. 3c and 3d) reveals that the metal agglomerates contain pores 50–500 nm in size, and individual particles are smaller than 50 nm.

When a similar mixture is combusted in nitrogen, the shape of synthesis products visually changes (Fig. 4). Combustion gives hollow spherical products varying in size and shape. The energy dispersive analysis of various spheres provides data on the presence of Ta, W, Mo, Hf, and Nb in a nearly equimolar proportion in all of them. The solid solution contains no nitrogen. The oxygen content is high, which is apparently due to intensive adsorption of oxygen on the developed surface of the particles. The morphology formed during combustion in nitrogen can be related to a change in the chemical potential of nitrogen

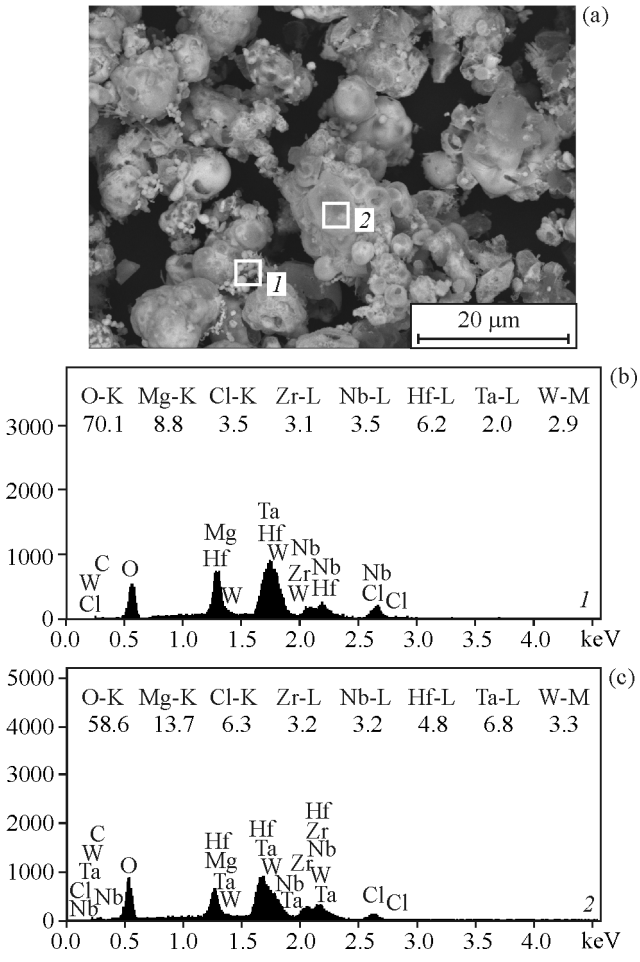

Fig. 4. Combustion products of the $TaCl_5 + ZrCl_4 + WCl_6 + HfCl_4 + NbCl_5 + 5Mg_3N_2$ mixture at 900°C in nitrogen.

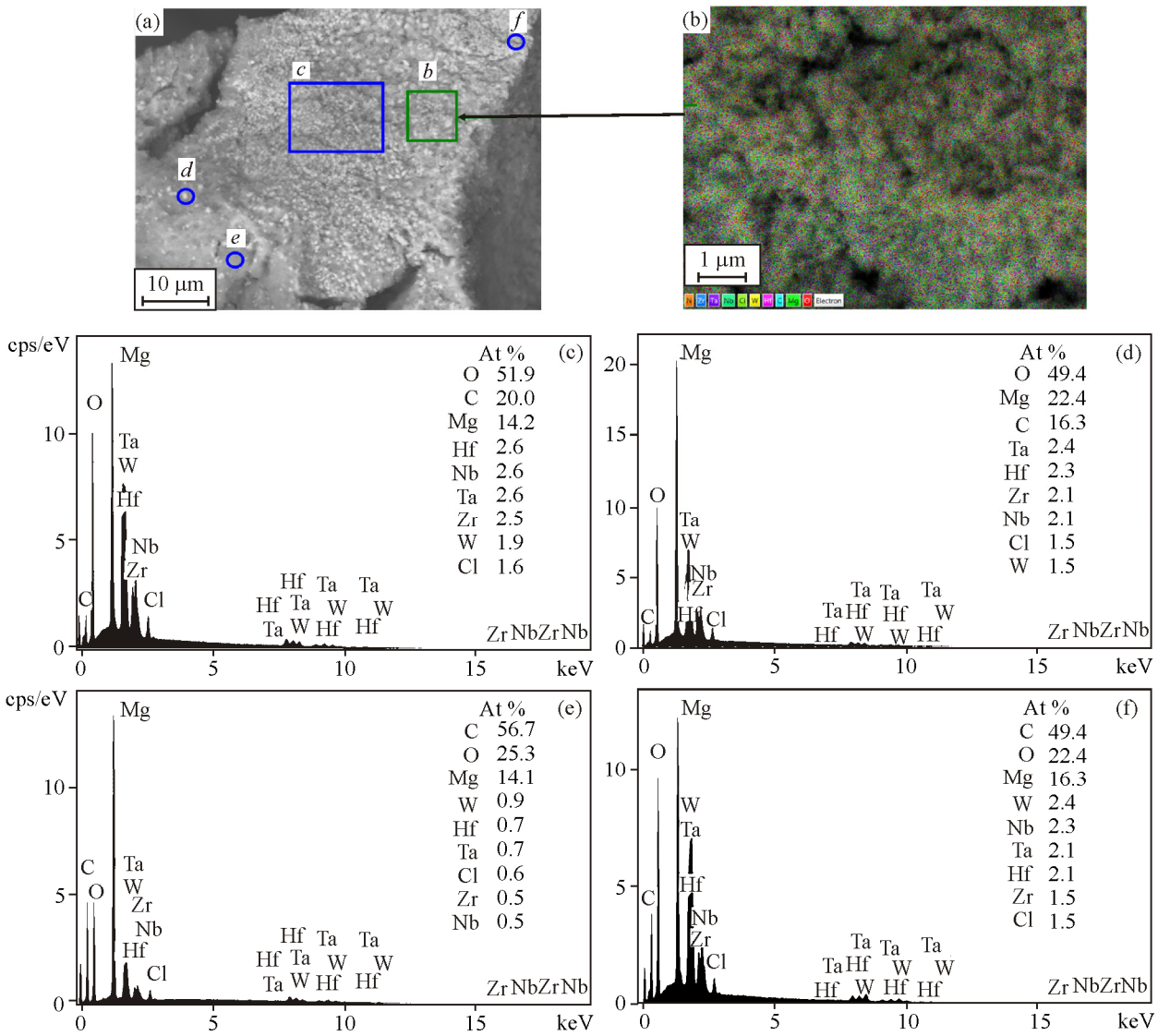

Fig. 5. Products of overall combustion of the ($TaCl_5 + ZrCl_4 + WCl_6 + HfCl_4 + NbCl_5 + 5Mg_3N_2$) gel at 900°C in nitrogen (color online).

when it has two sources: solid (magnesium nitride) and gaseous (atmosphere) ones.

3.3. Combustion of Chloride Reaction Mixtures in the Form of Ethanol-Based Gels

Gel combustion is a modification of the developed synthesis method. The necessity of using such combustion systems stems from the fact that conventional reducing agents (urotropine, cellulose, and glycine) are incapable of complete reduction of Group IV–VI metal ions. Although magnesium nitride is a solid-phase source of magnesium during combustion, no nitride phases form during such overall combustion of the reaction powder mixtures.

To prepare nitrides of Group IV–VI metals is of considerable interest. The preparation of high-entropy nitride compounds by solution combustion has not yet been described in the literature. However, mention was made of the fact that the addition of urotropine ($C_6H_{12}N_4$) to the solution as an additional source of nitrogen (in the form of highly reactive ammonia) and of a gel-forming agent stimulated the formation of nitrides.

The composition and morphology of combustion products are independent of the gaseous medium used for combustion (argon or nitrogen). According to Fig. 5a, they are composed of agglomerated nanoparticles of high-entropy nearly equimolar alloy (Figs. 5c, 5d, and 5f) relatively uniformly distributed

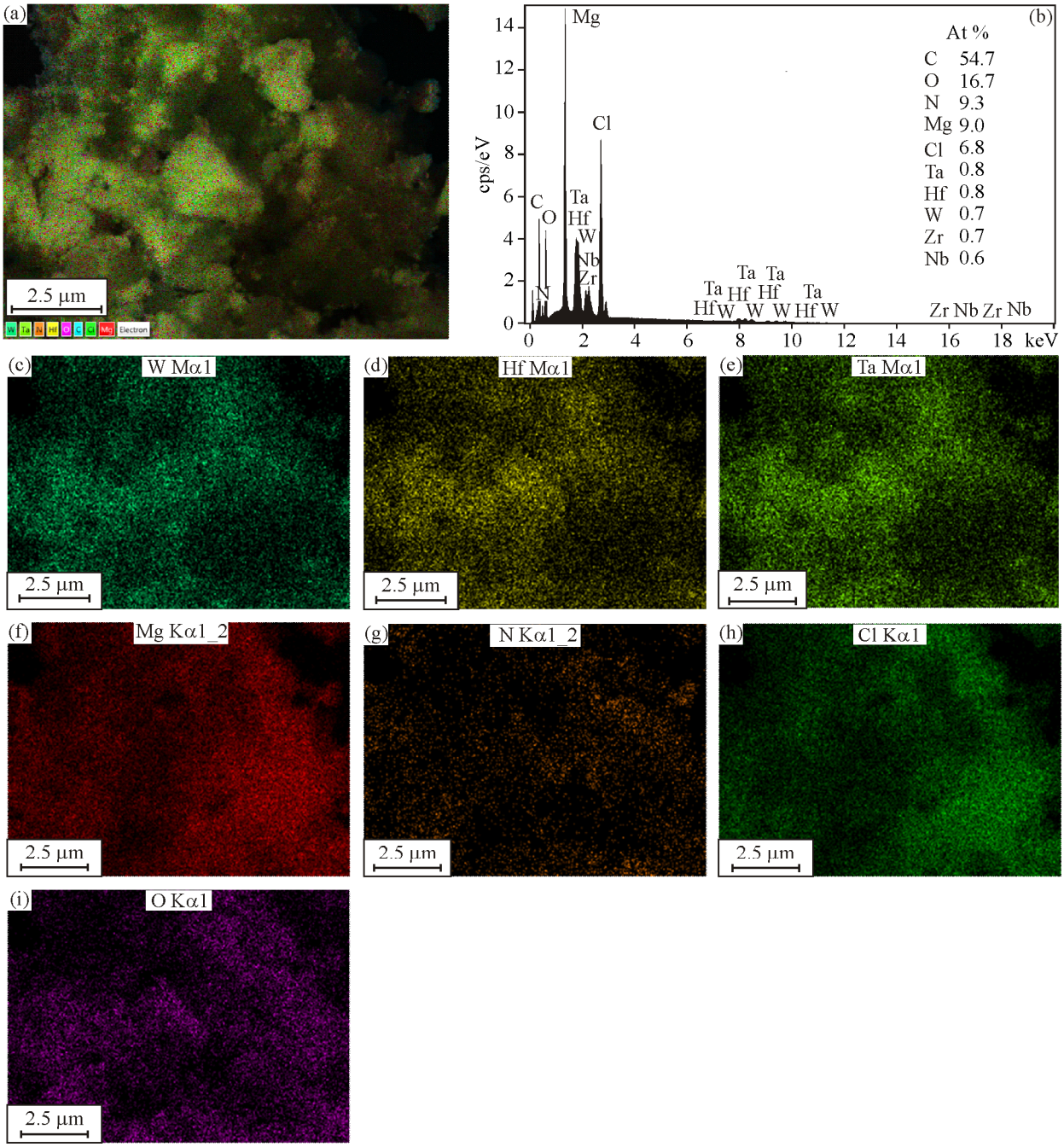

Fig. 6. Element distribution in products of overall combustion of the $TaCl_5 + ZrCl_4 + WCl_6 + HfCl_4 + NbCl_5 + 0.2C_6H_{12}N_4 + 5Mg_3N_2$ gel at 900°C in nitrogen (color online).

in the matrix of magnesium oxide (Fig. 5e). EDS maps of the combustion products (Fig. 5b) show the chemical homogeneity of the synthesized high-entropy alloy.

For the synthesis of high-entropy nitride, 0.2 mol of urotropine ($C_6H_{12}N_4$) is introduced into the gel. Its combustion yields products with a microstructure (Fig. 6) similar to that of the products obtained without urotropine (Fig. 5a). However, the EDS maps of the combustion products (Fig. 6) display a uniform distribution of the metal components and nitrogen in the light phase (Fig. 6a). The chemical composition integrated over maps (Fig. 6b) also indicates a high chemical homogeneity of the combustion products.

The large oxygen content in ethanol causes a rapid oxidation of the resulting nanoparticles (Fig. 7), which leads to the abundance of oxide phases.

The specific surface area of the powder obtained by pyrolysis of ethanol-based chloride gels without

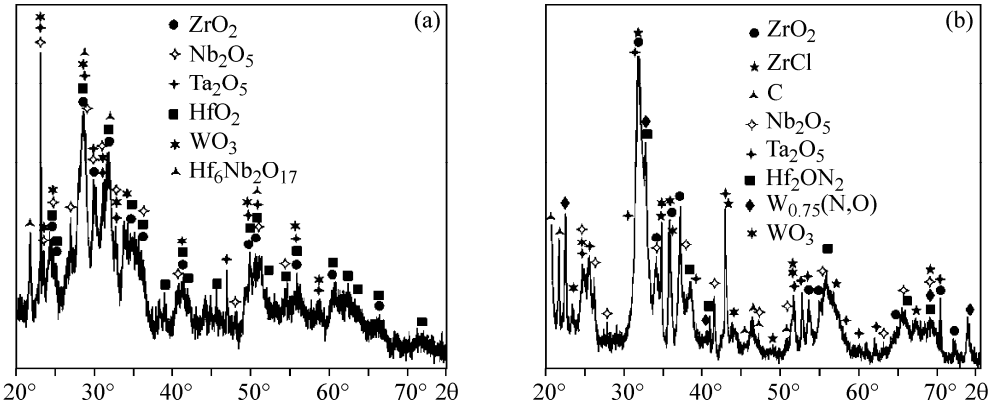

Fig. 7. Results of the X-ray phase analysis of powders pyrolyzed from ethanol-based chloride gels without (a) and with the introduction of urotropine (b).

urotropine (Fig. 7) is 14.4 m^2/g, while the powders synthesized with the addition of 0.2 mol of urotropine have a much smaller specific surface area (2.4 m^2/g), which is apparently due to high aggregation of nanoparticles.

4. CONCLUSIONS

We analyzed the stability of metallic, chloride, nitride and hydride phases for the Ta–Nb–Hf–Zr–W–Mg and Ta–Nb–Hf–Zr–W–Cl–Mg–N systems in the temperature interval 0–2000°C with varying chemical potentials of gaseous elements (chlorine and nitrogen).

Self-propagating high-temperature synthesis of magnesium nitride-chloride mixtures provides highly porous products, which consist of agglomerates of metal nanoparticles in the matrix of magnesium oxychloride. The use of magnesium nitride as the reducing agent results in the formation of needle-like particles of high-entropy Ta + Nb + Hf + Zr + W alloy.

The combustion of gels yields nanopowders with uniform composition and particle size, however a high reactivity of the synthesized nanopowders results in their rapid oxidation on account of a large amount of oxygen in the gel-forming agent. Thus, the method of production of high-entropy nitride ceramics requires further optimization.

FUNDING

The work was performed at the financial support of RFBR within Project No. 19-33-90124.

REFERENCES

1. Zhang, Y., Zuo, T.T., Tang, Z., Gao, M.C., Dahmen, K.A., Liaw, P.K., and Lu, Z.P., Microstructures and Properties of High-Entropy Alloys, *Prog. Mater. Sci*., 2014, vol. 61, pp. 1–93. https://doi.org/10.1016/j.pmatsci.2013.10.001
2. Dong, Y., Gao, X., Lu, Y., Wang, T., and Li, T., A Multi-Component $AlCrFe_2Ni_2$ Alloy with Excellent Mechanical Properties, *Mater. Lett*., 2016, vol. 169, pp. 62–64. https://doi.org/10.1016/j.matlet.2016.01.096
3. He, J.Y., Wang, H., Huang, H.L., Xu, X.D., Chen, M.W., Wu, Y., Liu, X.J., Nieh, T.G., An, K., and Lu, Z.P., A Precipitation-Hardened High-Entropy Alloy with Outstanding Tensile Properties, *Acta Mater*., 2016, vol. 102, pp. 187–196. https://doi.org/10.1016/j.actamat.2015.08.076
4. Li, D. and Zhang, Y., The Ultrahigh Charpy Impact Toughness of Forged $Al_xCoCrFeNi$ High Entropy Alloys at Room and Cryogenic Temperatures, *Intermetallics*, 2016, vol. 70, pp. 24–28. https://doi.org/10.1016/j.intermet.2015.11.002
5. Yu, P.F., Cheng, H., Zhang, L.J., Zhang, H., Ma, M.Z., Li, G., Liaw, P.K., and Liu, R.P., Nanotwin's Formation and Growth in an AlCoCuFeNi High-Entropy Alloy, *Scripta Mater*., 2016, vol. 114, pp. 31–34. https://doi.org/10.1016/j.scriptamat.2015.11.032
6. Praveen, S., Basu, J., Kashyap, S., and Kottada, R.S., Exceptional Resistance to Grain Growth in Nanocrystalline CoCrFeNi High Entropy Alloy at High Homologous Temperatures, *J. Alloys Compd*., 2016, vol. 662, pp. 361–367. https://doi.org/10.1016/j.jallcom.2015.12.020
7. Zhu, G., Liu, Y., and Ye, J., Fabrication and Properties of Ti(C,N)-Based Cermets with Multi-Component AlCoCrFeNi High-Entropy Alloys Binder, *Mater. Lett*., 2013, vol. 113, pp. 80–82. https://doi.org/10.1016/j.matlet.2013.08.087
8. Chen, C.-S., Yang, C.-C., Chai, H.-Y., Yeh, J.-W., and Chau, J.L.H., Novel Cermet Material of WC/Multi-Element Alloy, *Int. J. Refract. Met. Hard Mater*., 2014, vol. 43, pp. 200–204. https://doi.org/10.1016/j.ijrmhm.2013.11.005

9. Guo, N.N., Wang, L., Luo, L.S., Li, X.Z., Chen, R.R., Su, Y.Q., Guo, J.J., and Fu, H.Z., Microstructure and Mechanical Properties of In-Situ MC-Carbide Particulates-Reinforced Refractory High-Entropy $Mo_{0.5}$Nb Hf+ZrTi Matrix Alloy Composite, *Intermetallics*, 2016, vol. 69, pp. 74–77. https://doi.org/10.1016/j.intermet.2015.09.011
10. Khaliullin, S.M., Zhuravlev, V.D., Bamburov, V.G., Khort, A.A., Roslyakov, S.I., Trusov, G.V., and Moskovskikh, D.O., Effect of the Residual Water Content in Gels on Solution Combustion Synthesis Temperature, *J. Sol-Gel Sci. Technol*., 2020, vol. 93. https://doi.org/10.1007/s10971-019-05189-8
11. Jin, T., Sang, X., Unocic, R.R., Kinch, R.T., Liu, X., Hu, J., Liu, H., and Dai, S., Mechanochemical-Assisted Synthesis of High-Entropy Metal Nitride via a Soft Urea Strategy, *Adv. Mater*., 2018, vol. 30, p. 1707512. https://doi.org/10.1002/adma.201707512
12. Yermekova, Z., Roslyakov, S., Trusov, G., Leybo, D., Bindiug, D., and Mukasyan, A., Optimization of the Fabrication Parameters of the Co_3O_4/SiO_2 Supported Ceramic Catalyst for CO Gas Conversion: Design of Experiment for Solution Combustion Synthesis, *Ceram. Int*., 2021, vol. 47, pp. 12935–12940. https://doi.org/10.1016/j.ceramint.2021.01.156
13. Mukasyan, A.S., Moskovskikh, D.O., Nepapushev, A.A., Pauls, J.M., and Roslyakov, S.I., Ceramics from Self-Sustained Reactions: Recent Advances, *J. Eur. Ceram. Soc*., 2020, vol. 40. https://doi.org/10.1016/j.jeurceramsoc.2019.12.028
14. Parauha, Y.R., Sahu, V., and Dhoble, S.J., Prospective of Combustion Method for Preparation of Nanomaterials: A Challenge, *Mater. Sci. Eng. B*, 2021, vol. 267, p. 115054. https://doi.org/10.1016/j.mseb.2021.115054
15. Varma, A., Mukasyan, A.S., Rogachev, A.S., and Manukyan, K.V., Solution Combustion Synthesis of Nanoscale, *Mater. Chem. Rev*., 2016, vol. 116, pp. 14493–14586. https://doi.org/10.1021/acs.chemrev.6b00279
16. Khort, A., Podbolotov, K., Serrano-García, R., and Gun'ko, Y., One-Step Solution Combustion Synthesis of Cobalt Nanopowder in Air Atmosphere: The Fuel Effect, *Inorg. Chem*., 2018, vol. 57, pp. 1464–1473. https://doi.org/10.1021/acs.inorgchem.7b02848
17. Yermekova, Z., Roslyakov, S.I., Kovalev, D.Y., Danghyan, V., and Mukasyan, A.S., One-Step Synthesis of Pure γ-FeNi Alloy by Reactive Sol-Gel Combustion Route: Mechanism and Properties, *J. Sol-Gel Sci. Technol*., 2020, vol. 94, pp. 310–321. https://doi.org/10.1007/s10971-020-05252-9
18. Khort, A., Romanovski, V., Leybo, D., and Moskovskikh, D., CO Oxidation and Organic Dyes Degradation Over Graphene–Cu and Graphene–CuNi Catalysts Obtained by Solution Combustion Synthesis, *Sci. Rep.*, 2020, vol. 10, p. 16104. https://doi.org/10.1038/s41598-020-72872-0